Zhang *et al.*
Progress in Earth and Planetary Science (2025) 12:32
https://doi.org/10.1186/s40645-025-00702-w

Progress in Earth and Planetary Science

RESEARCH ARTICLE

Open Access

Stability and water solubility of calcium ferrite-type aluminum-rich phase: implications for deep water cycle caused by subducting basaltic crusts

Xinyue Zhang[1,2], Izumi Mashino[2] and Takayuki Ishii[2*]

Abstract

The subducting crustal materials serve as a crucial channel for transporting water to the lower mantle. Recent experimental studies suggest that crustal materials such as basaltic crust can be a main water carrier and reservoir playing an important role on water cycling in the lower mantle. Despite being a primary mineral in crustal materials, the water solubility of calcium ferrite-type (CF) phase and its stability are unclear yet. A recent phase relation study of hydrous basalts showed Na-depletion in lower-mantle minerals, suggesting the presence of fluid possibly with high Na concentration and the absence of CF phase along the low-temperature slab geotherms, where Al-rich hydrous phase H and ferropericlase appear instead. These phases could consequently produce Na-depleted CF phase when reaching the dehydration temperature of Al-rich hydrous phase H. In this study, we investigated the stability and water solubility of CF-type $MgAl_2O_4$, which is a main CF component in a hydrous basalt, in water-bearing systems at 26–32 GPa and 1200–1900 °C using a Kawai-type multi-anvil press. Our results indicate that the stability of the CF phase is strongly influenced by water content in the system. Water contents of recovered CF phases estimated by Fourier-transform infrared spectroscopy show a limited variation between 73 and 87 ppm wt at a pressure of 26 GPa and temperatures of 1500–1900 °C. We suggest that CF phase could not be a primary water carrier at lower mantle depths. This emphasizes contributions of hydrous aluminous silica minerals to Earth's deep water cycling and heterogeneous structures in the lower mantle due to the strong water partitioning to this phase compared with other constituent minerals.

Keywords Water solubility, CF phase, Single crystal, FTIR, MORB

*Correspondence:
Takayuki Ishii
takayuki.ishii@okayama-u.ac.jp
[1] Deep Space Exploration Laboratory/School of Earth and Space Sciences, University of Science and Technology of China, Hefei 230026, Anhui, China
[2] Institute for Planetary Materials, Okayama University, Misasa, Tottori 682-0193, Japan

1 Introduction

The subducted slab plays an important role in the water and material cycles in the Earth's interior (Bercovici and Karato 2003; Nishi et al. 2014; Andrault and Bolfan-Casanova (2022) Keppler et al. 2024; Ohtani and Ishii 2024). How water is transported by the subducting slab into and distributed in the deep mantle is crucial to understand structure and dynamics of the mantle because water significantly impacts the physical properties of mantle minerals such as melting temperature, elasticity, electrical/thermal conductivities, and rheology (Green et al. 2014; Kohlstedt 2006; Mao et al. 2008; Marzotto et al. 2020; Wang et al. 2006). Discovery of hydrous ringwoodite as diamond inclusion reveals presence of water at least down to the mantle transition zone (Pearson et al. 2014). Geochemical observations of ocean island basalts suggest water-rich sources in the lower mantle (e.g. Hirschmann 2006). However, water transport and capacity in the lower mantle remain unclear.

One open question is the water hosts in the lower mantle. The two most abundant minerals in a pyrolitic lower mantle (Irifune et al. 2010; Ishii et al. 2011, 2018a), bridgmanite and ferropericlase, have very limited water storage capacity up to ~1000 and ~100 ppm wt, respectively (Bolfan-Casanova et al. 2003; Fu et al. 2019; Liu et al. 2021). The water content of davemaoite, the third abundant phase (~ 8 vol.%) in a pyrolitic lower mantle (Irifune et al. 2010; Ishii et al. 2011, 2018a; Nishiyama and Yagi 2003), is still under debate but possibly 0.4–1 wt% (Chen et al. 2020; Murakami et al. 2002). In addition to the minerals in pyrolite, subducted crustal materials such as basalt and continental crusts/sediments feature completely different mineral assemblages due to their distinct compositions. In addition to bridgmanite and davemaoite, the higher contents of SiO_2 and Al_2O_3 in these compositions stabilize silica phases such as stishovite and $CaCl_2$-type post-stishovite as well as Al-rich phases such as calcium ferrite-type (CF) phase and the new hexagonal aluminous phase (NAL), at lower-mantle depths (Irifune et al. 1994; Ishii et al. 2012, 2019, 2022c; Ono et al. 2001; Perrillat et al. 2006; Ricolleau et al. 2010). The water content of stishovite is significantly influenced by its alumina content, which is less than 521 ppm wt in Al-free system but could reach up to ~0.3 wt% in Al-bearing systems, which is a more realistic system in crustal materials (Ishii et al. 2022b; Litasov et al. 2007; Purevjav et al. 2024). $CaCl_2$-type post-stishovite can accommodate even more water, up to 1.1 wt% (Ishii et al. 2022b).

On the other hand, there is a paucity of research on the water content of Al-rich phases, mainly caused by their questionable stability in a hydrous system (Ishii et al. 2023a; Liu et al. 2019). Recent studies have found no CF phase under hydrous conditions (Ishii et al. 2023a; Liu et al. 2019). In hydrous basalt systems with 2–3.5 wt% H_2O at 17–26 GPa and 800–1200 °C, CF and NAL phases were not observed but Al-rich phase H appears as an alumina host phase together with ferropericlase and fluid (Liu et al. 2019). A recent phase relation study in a $NaAlSiO_4$-$MgAl_2O_4$-Fe_3O_4-H_2O system reported that no CF phase appears in the hydrous system at 24 GPa up to 2000 °C, where Al-rich hydrous phase δ and Fe-rich hydrous phase ε or corundum appear together with stishovite and Na-rich melt depending on temperature (Ishii et al. 2023a). One of the reasons for the absence of CF phase can be attributed to the reduced stability of CF phase in Na-bearing environments due to Na partitioning into hydrous melt under a relatively large amount of water in the system (~ 11 wt%) (Ishii et al. 2023a). Although no chemical composition of fluid was reported in the hydrous basaltic system (Liu et al. 2019), it is inferred to contain a large amount of Na (Ishii et al. 2023a). This is also supported by the significantly low Na concentrations in mineral assemblages under lower mantle conditions (Liu et al. 2019), which suggests a strong Na partitioning into fluid, a phenomenon not observed in the dry basaltic system (Ishii et al. 2019) (Supplementary material 1: Fig. S1).

Another reason would be due to low temperature synthesis conditions. Liu et al. (2019) determined phase stability in the hydrous basalt system only up to 26 GPa and 1200 °C, where Al-rich hydrous phase H is thermally stable (Ishii et al. 2022 d). As the temperature of a subducting slab, especially in the top layer of a basaltic crust, will increase with time due to the high temperature of the average lower mantle, the following reaction can be expected after dehydration of Al-rich hydrous phase H:

$$\begin{aligned} &2(\mathrm{Mg,Fe})_n\mathrm{Si}_n(\mathrm{Al,Fe})_{1-2n}\mathrm{OOH\ Al-rich\ phase}\ H \\ &+(1-2n)(\mathrm{Mg,\ Fe})\mathrm{O\ ferropericlase} \\ &\rightarrow (\mathrm{Mg,Fe})\left(\mathrm{Si}_n(\mathrm{Al,Fe})_{1-2n}\right)_2\mathrm{O}_4\ \mathrm{CF\ phase} \\ &\pm\ \mathrm{hydrous\ fluid/melt} \end{aligned}$$

Na-rich fluids formed in the low-temperature mineral assemblage (the right side) are likely released from the basaltic layer due to their possible low density (Hack and Thompson 2011). The presence of hydrous fluid/melt depends on the water solubility of Na-depleted CF phase. The presence of fluid can cause rehydration of mantle minerals and formation of heterogeneous mantle structures, for example, seismic scatterers observed in the lower mantle (Ohtani and Ishii 2024), emphasizing the necessity to investigate the stability and water solubility of Na-depleted CF phase across varying water content.

In this study, we attempted to synthesize the high-quality single-crystal CF phase in $MgAl_2O_4$-H_2O systems, which is

one of the most abundant components in CF phase based on the above discussion, by using multi-anvil techniques at temperatures of 1200–1900 °C and pressures of 26–32 GPa. The water solubility of CF phase was carefully examined using recovered single crystals by Fourier-transform infrared spectroscopy (FTIR). Based on our results, heterogeneous structures and water cycling in the lower mantle will be discussed.

2 Experiment

To synthesize CF phase in hydrous systems, high-pressure and high-temperature experiments were conducted at 26–32 GPa and 1200–1900 °C for 3–7 h using the 1000-ton and 5000-ton Kawai-type multi-anvil apparatus (USSA-1000 and -5000, respectively) installed at the Institute for Planetary Materials (IPM), Okayama University, Japan. Mixtures of MgO, Al_2O_3, and $Al(OH)_3$ powders or synthetic $MgAl_2O_4$ spinel (Ishii et al. 2021), MgO, and $Al(OH)_3$ powders were prepared as the starting materials in the $MgAl_2O_4$−5 wt% H_2O and $MgAl_2O_4$−10 wt% H_2O systems. Regent-grade MgO, Al_2O_3, and $Al(OH)_3$ powders were heated at 1000 °C, 500 °C, and 150 °C, respectively, to remove adsorbed water just before weighing. For the experiments conducted below 27 GPa, the starting mixtures were packed in welded Pt-tube capsules with two Pt disks at both ends. A Cr-doped MgO octahedron with 8-mm edge length served as pressure medium. Two types of tungsten carbide (WC) anvils with 3-mm truncations, F08 and F05 grades (Fuji Die Co., Ltd.), were used in our experiments. A cylindrical $LaCrO_3$ heater with two lids at both ends was inserted into the center of the octahedron. An MgO sleeve with two lids were located inside the heater to electrically insulate the samples from the heater. For the experiments conducted at 32 GPa, the concept of the cell design was adopted to that reported in Ishii et al. (2017) and Ishii et al. (2016). The starting mixtures were packed in a Pt-foil capsule, which was inserted into a Mo-foil heater. Mo-rod electrodes were located at both ends of the heater. A ZrO_2 sleeve was wrapped around the Mo heater. WC anvils with 1.5-mm truncations (F05 grade) were used with a 6-mm edge length Cr-doped MgO octahedron as pressure medium. Pressure calibration was conducted at 2000 K using phase transitions from ringwoodite to bridgmanite + periclase (Chanyshev et al. 2022), pyrope to bridgmanite + corundum (Ishii et al. 2023b) and compositions of aluminous bridgmanite coexisting with corundum (Liu et al. 2017) in separate runs. Temperature was monitored at the surface of the sample capsule using a $W_{97\%}Re_{3\%}$-$W_{75\%}Re_{25\%}$ thermocouple. The samples were first compressed to a desired press load (7.0–8.5 MN corresponding to 26–32 GPa), and then heated to 1200–1900 °C at a rate of 50 °C/min. The target temperature was maintained for the specified duration of 3–7 h before the samples were quenched by cutting the electric power supply and subsequently decompressed to ambient pressure over a period of 12 h.

The recovered capsules were embedded in epoxy resin and polished for the subsequent analysis. Phase identification of the samples was performed using a micro-focus X-ray diffractometer (RINT RAPID II, RIGAKU Co., Japan) with an imaging plate. The operating conditions were 40 kV and 30 mA with a Cu target X-ray source and collimator size of 100 μm. Microstructural observations were conducted using a field-emission-type scanning electron microscope (SEM) (JSM-7001 F, JEOL Co., Japan) with operating conditions of 15-kV accelerating voltage and 15-nA beam current. The chemical compositions were analyzed using a field-emission-type electron probe microanalyser (EPMA) (JEOL JXA8800) with operating conditions of 15 kV and 1 nA or 5 nA. Crystals of the CF phase, identified by their light orange color and elongated columnar morphology, were extracted from the capsules. Polarizing microscopes were utilized to confirm that the selected fragments were single crystals. Raman spectroscopy was subsequently performed using a modular Raman spectrometer (HORIBA Scientific iHR550-FIBMIC-DE-BXFM) to further characterize these single crystals. Raman spectra were collected between 150–1200 cm^{-1} frequency range with a green 532 nm diode-pumped solid-state laser for 60 s and 3 accumulations. Note that large crystals of CF phases found in the recovered samples (1k3791, 1k3814, and 1k3816) (Table 1) were picked up without surface observations using the SEM to avoid loss of crystals for FTIR measurements. Instead, we confirmed phases of the aggregate in selected regions (high and low temperature parts) by micro-focus X-ray diffraction.

Water contents of the recovered samples were determined using a FTIR spectrometer (JASCO FT/IR-6600 and IRT-5200IPMY) with an aligned transmission geometry under vacuum conditions at IPM. Single crystals of CF phase with a random orientation were double-polished to thicknesses of 30–90 μm and placed on a KBr single-crystal plate for unpolarized FTIR measurements. FTIR spectra were obtained using an unpolarized IR beam with an aperture size of 25×25 μm^2, averaging 256 scans with a resolution of 4 cm^{-1}. The water content was calculated using the empirical formulation of Paterson (1982), which is shown as follows:where C_{OH} represents the concentration of water in ppm wt, ζ is an orientation factor of 1/3 for unpolarized spectra, $K(\overline{\nu})$ is the absorption coefficient in cm^{-1} for a given wavenumber $\overline{\nu}$, and

X_i is the density factor defined as $X_i = 10^6 \times (18/2d)$, where d is the mineral density of 3.937 g/cm^3 for CF phase and 3.987 g/cm^3 for corundum (Irifune et al. 1991; Zhang et al. 2024). FTIR spectra were integrated between 3000 and 3780 cm^{-1}.

$$C_{OH} = \frac{X_i}{150\zeta} \int \frac{K(\overline{\nu})}{(3780-\overline{\nu})} d\overline{\nu} \quad (1)$$

3 Results and discussion

3.1 Run Products and the phase stability of CF phase

The experimental conditions and run products are summarized in Table 1. The hydrous melt was found in the capsules synthesized at 1700–1900 °C (Fig. 1), suggesting a water-saturated condition. In the run 1k3791 conducted at 26 GPa and 1700 °C, we examined the effect of water contents in the starting materials on CF phase stability. Two starting materials with 5 wt% and 10 wt% H_2O were placed symmetrically in a high-pressure cell, but the resulting products differed significantly between the two systems (Supplementary material 1: Fig. S2). The products in the 5-wt%-H_2O system were primarily identified through X-ray diffraction, revealing the main phase was CF phase, accompanied by small amounts of corundum and periclase (Fig. 2; Supplementary material 1: Table S1). Upon opening the capsule, MgO-rich hydrous fluid was observed on the high temperature side (Table S1). The appearance of corundum and periclase at the low temperature side can be explained by the negative phase boundary between CF phase and corundum plus periclase, which lies near the pressure–temperature conditions of our experiments (Irifune et al. 2002). Conversely, in the 10-wt%-H_2O system, the primary phases were corundum and periclase, with no CF phase in XRD spectra and back-scattered electron images (Figs. 1 and 2). Magnesia-rich hydrous fluid and corundum were also shown at the hotter ends of the capsules, while small brucite inclusions existed in the single crystal of corundum (Figs. 1 and 2). Relatively large periclase grains were located next to the large corundum grains. A fine mixture of periclase and corundum or δ-AlOOH were shown at the low temperature end. Our results indicate that the CF phase is unstable when the water content in the system exceeds 10 wt%, which is consistent with the previous phase relation study in the system $NaAlSiO_4$-$MgAl_2O_4$-Fe_3O_4 with 11 wt% water (Ishii et al. 2023a), even though no sodium component were included in this study. Thus, we found that water content in a system significantly influences the stability of CF phase. This is probably due to high concentrations of elements consisting of CF phase into the hydrous melt such as Mg and Na, remaining SiO_2 and Al_2O_3 phases.

Subsequent experiments focused on the 5-wt%-H_2O system to examine the influence of temperature and pressure on the stability of CF phase and to obtain CF phase crystals. In the run 5k4199 conducted at 27 GPa and 1200 °C, no CF phase appeared, while the mixture of δ-AlOOH, corundum, and periclase was shown in the capsule (Figs. 3 and 4). When increasing the pressure to 32 GPa (5k4209), a mineral assemblage of CF phase, δ-AlOOH, and periclase became stable. The same phase change also happened in the experiments conducted at 1400 °C and 26 (1k3801) and 27 GPa (5k4195). At 27 GPa and 1400 °C, CF phase coexisted with δ-AlOOH, periclase, and corundum, indicating that this condition was quite close to the reaction boundary between CF phase and periclase and corundum. At 26 GPa and 1500 (1k3814) and 1900 °C (1k3816), CF phase crystals with dimensions of 50–400 μm were found coexisting with periclase + δ-AlOOH and corundum + hydrous melt, respectively (Figs. 3 and 5). The compositions of hydrous melt in the recovered capsule were also magnesia-rich at 1900 °C (Table S1).

Table 1 Details of the synthesis conditions and run products

Run No	Starting material	Temperature (°C)	Pressure (GPa)	Duration (h)	Products at HT	Products at LT
1k3791	$MgAl_2O_4$–5 wt% H_2O	1700	26	3	CF + Cor + L	CF + Cor + Per
	$MgAl_2O_4$–10 wt% H_2O	1700	26	3	Cor + Per + L + Bru*	Cor + Per + δ
1k3814	$MgAl_2O_4$–5 wt% H_2O	1500	26	6	CF + δ + Per	δ + Per + Cor
1k3816	$MgAl_2O_4$–5 wt% H_2O	1900	26	3	CF + Cor + L	CF + Cor + Per
1k3801	$MgAl_2O_4$–5 wt% H_2O	1400	26	5.5	Cor + Per + δ + Mag‡	
5k4195	$MgAl_2O_4$–5 wt% H_2O	1400	27	3	CF + δ + Per + Cor + Mag‡	
5k4199	$MgAl_2O_4$–5 wt% H_2O	1200	27	7	Cor + Per + δ + Mag‡	
5k4209	$MgAl_2O_4$–5 wt% H_2O	1200	32	3	CF + δ + Per + Mag‡	

Note. CF = calcium ferrite-type phase; Cor = corundum; Per = periclase; δ = δ-AlOOH phase; Bru = brucite; Mag = magnesite; L = melt; HT = high-temperature part; LT = low-temperature part

* Brucite might be a quenched phase

‡ Minor amounts were found probably due to a small exchanging reaction of brucite to magnesite by air in the starting materials

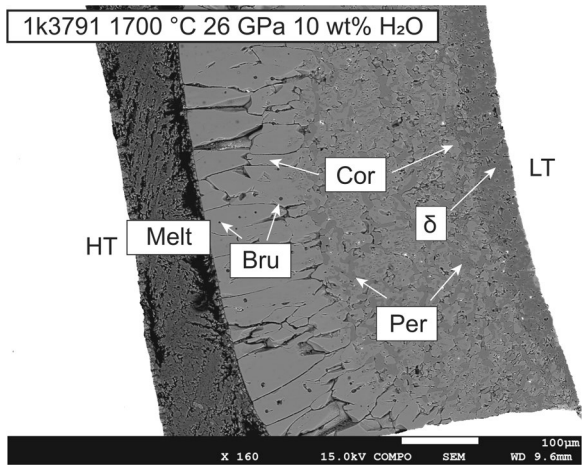

Fig. 1 A back-scattered electron image of recovered products synthesized at 1700 °C and 26 GPa (run 1k3791) with 10 wt% H_2O. Cor = corundum; Per = periclase; δ = δ-AlOOH phase; Bru = brucite; HT = high-temperature part; LT = low-temperature part

Using the results at 26–27 GPa and 1200–1500 °C, the phase boundary between CF phase and corundum + periclase was drawn and showed a slope of −7 MPa/°C (Supplementary material 1: Fig. S3). Irifune et al. (2002) determined a gentler negative slope of (−2 MPa/°C) near 25 GPa by in-situ multi-anvil experiments in combination with Anderson's Au pressure scale (Anderson et al. 1989). However, it is known that Anderson's scale underestimates pressure, compared with more recent Au scales such as Tsuchiya's and Yokoo's Au scales, showing ~ 1 GPa higher values around top-lower mantle conditions (Tsuchiya 2003; Yokoo et al. 2009). Adjusting for newer scales, the transition pressure at 1200 °C reported by Irifune et al. (2002) would shift to ~ 27 GPa. Note that quench experiments showed a larger negative slope of −4 MPa/°C (Akaogi et al. 2024; Enomoto et al. 2009). On the other hand, thermodynamic calculation with calorimetric data places the transition pressure at 29 GPa and 1200 °C with a relatively steep negative slope (−6 MPa/°C) (Kojitani et al. 2012a). Ishii et al. (2022a) argued that phase boundaries determined by high-pressure experiments may not be accurate without careful confirmation of stable phases due to possible kinetic problems and pressure drop during heating. These errors may have made a smaller slope by Irifune et al. (2002). This might be a reason that no CF phase appeared at 27 GPa and 1200 °C in this study. Thus, the phase boundary may be a steeper slope than that of the previous multi-anvil study although further study is needed due to limited data. Note that the present system is under hydrous

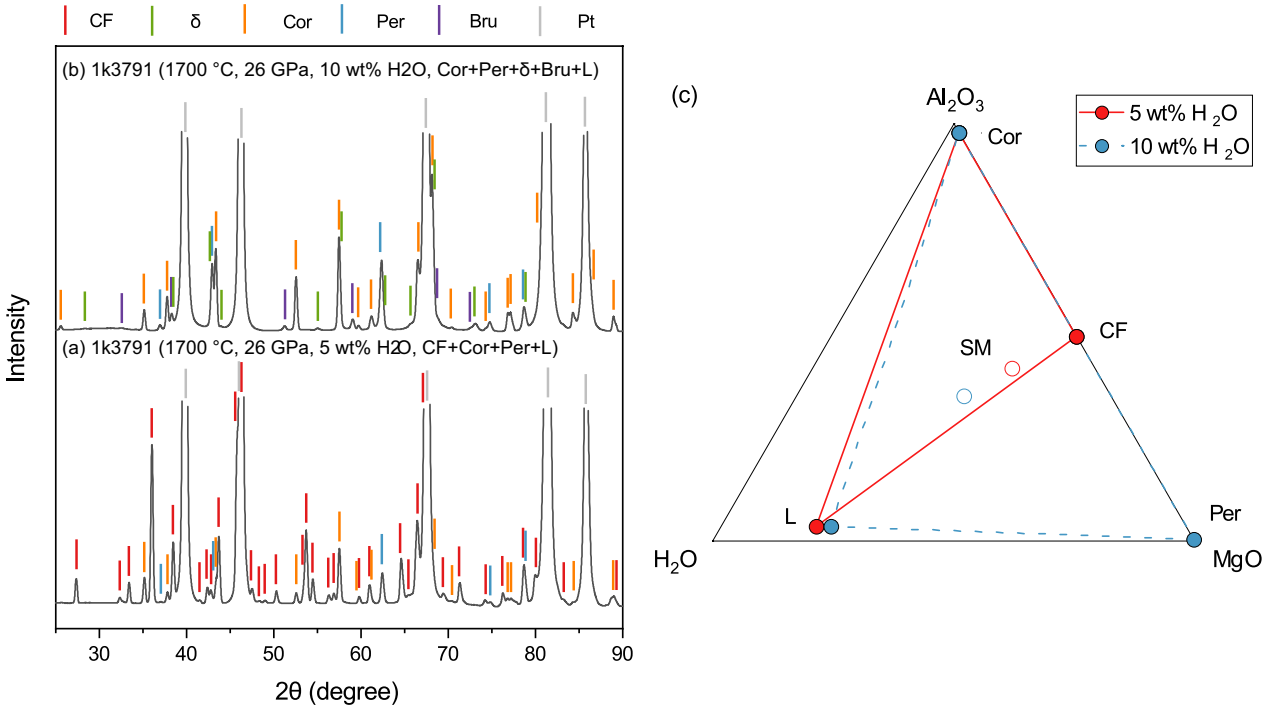

Fig. 2 XRD profiles and phase diagrams of the recovered samples from run 1k3791 at 26 GPa and 1700 °C. (**a**) 5 wt% H_2O system; (**b**) 10 wt% H_2O system; (**c**) Phase diagrams in MgO-Al_2O_3-H_2O ternary systems. CF = calcium ferrite-type phase; Cor = corundum; Per = periclase; δ = δ-AlOOH phase; Bru = brucite; L = melt; SM = starting material

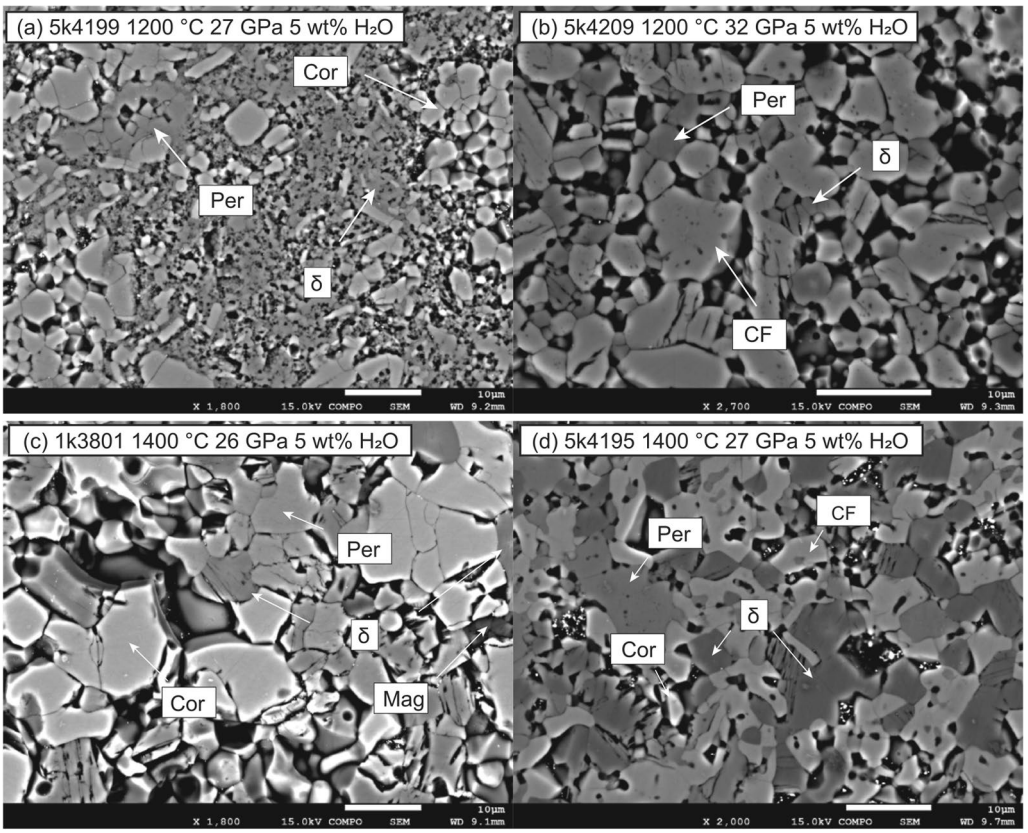

Fig. 3 Back-scattered electron images of recovered products synthesized at different conditions with 5 wt% H_2O. (**a**) 5k4199 at 1200 °C and 27 GPa; (**b**) 5k4209 at 1200 °C and 32 GPa; (**c**) 1k3801 at 1400 °C and 26 GPa; (**d**) 5k4195 at 1400 °C and 27 GPa. CF = calcium ferrite-type phase; Cor = corundum; Per = periclase; δ = δ-AlOOH phase; Mag = magnesite

conditions. The stabilization of δ-AlOOH + periclase can also shift the CF stability to higher pressures.

3.2 Characterization of CF phase single crystals

Recovered CF crystals synthesized at 26 GPa and 1500–1900 °C were characterized by micro-Raman spectroscopy. Raman spectra of CF phase displayed 12–17 peaks at 150–850 cm^{-1}, depending on the orientation (Fig. 6). All the peaks were assigned to the CF phase based on the reported vibrational bands (Kojitani et al. 2003, 2012b). The total cation occupancies of Mg and Al in CF phase were 1.01–1.03 and 1.97–1.99, respectively, which are consistent with the expected stoichiometry (Table S1). Because the total cation number is more than 3, an oxygen vacancy component could be included. Small amounts of Si were detected in all crystals, suggesting 0.2–0.7 mol% Mg_2SiO_4 component. This is likely due to minor contamination from the agate mortar at the sample grinding process.

Unpolarized FTIR spectra of CF phase single crystals showed several OH bands. The CF phase exhibited seven sharp OH peaks at 3441, 3470, 3500, 3510, 3616, 3660, and 3695 cm^{-1} (Fig. 7, Supplementary material 1: S4 and S5). Notably, the peak at 3695 cm^{-1} is often observed in the FTIR spectra of bridgmanite and ferropericlase, attributed to the inclusion of brucite (Bolfan-Casanova et al. 2003; Litasov et al. 2003; Litasov 2010). To distinguish the influence of brucite inclusion, we measured different positions within each single crystal. In one crystal synthesized at 1900 °C, the intensity of the peak at 3695 cm^{-1} varied significantly across different areas, while the intensity of other peaks remained nearly constant (Supplementary material 1: Fig. S6). However, brucite was not detected by X-ray diffraction nor Raman spectroscopy in the single crystal, suggesting that any such peaks were probably below detection limit. Some crystals exhibit one or two broad bands around 3000–3400 cm^{-1}. These bands are not consistently present across all crystals, and their positions and intensities vary between crystals and different regions in one crystal (Supplementary material 1: Fig. S5 and S6). Although the origin of these bands is unclear, the calculation for the water contents included them. We also measured the FTIR spectrum of single-crystal corundum from the recovered capsules, identifying a broad band near ~3000 cm^{-1} with maxima at 2983 and 3051 cm^{-1} and a weaker peak at 3270 cm^{-1}, along with several bands below 2600 cm^{-1}. These features are

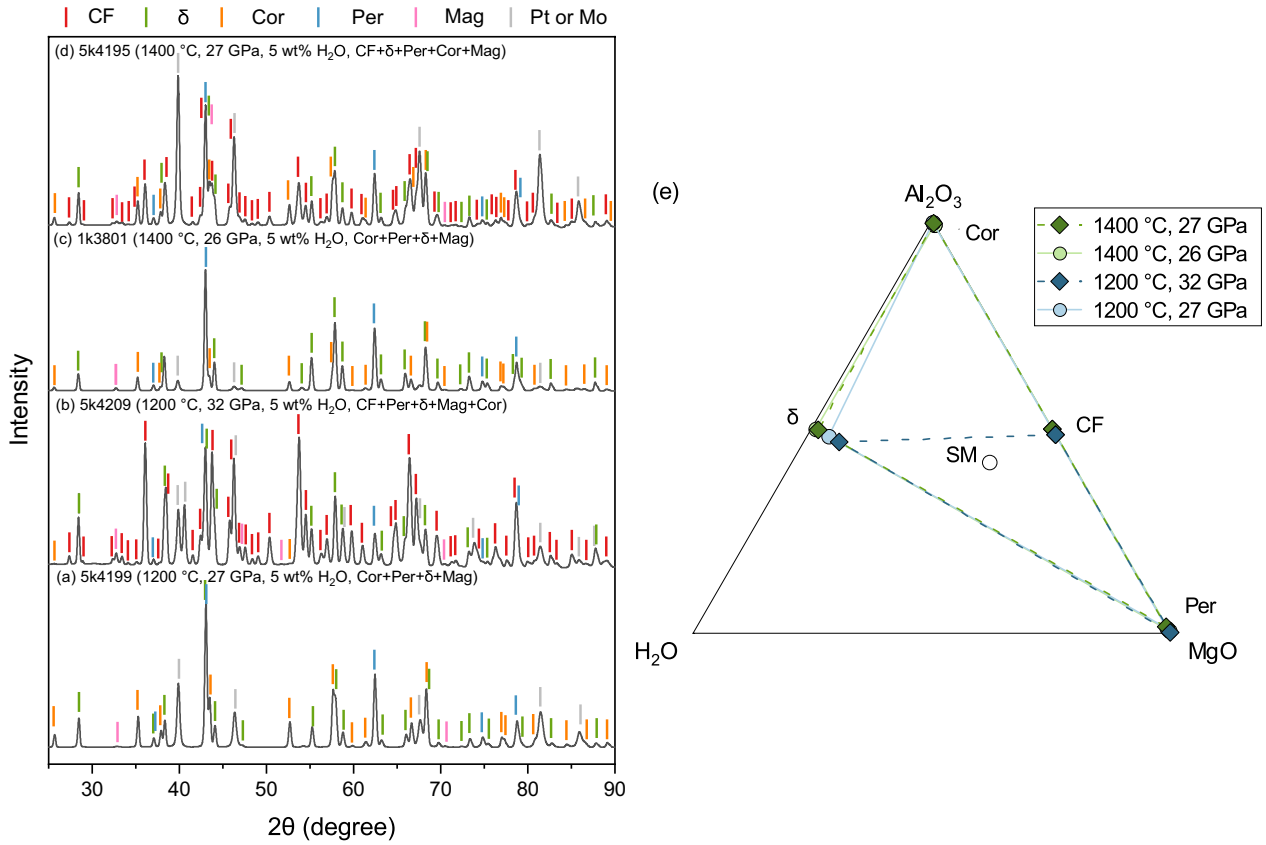

Fig. 4 XRD profiles and phase diagrams of the recovered samples from different runs in the 5 wt% H_2O system. (**a**) 5k4199 at 1200 °C and 27 GPa; (**b**) 5k4209 at 1200 °C and 32 GPa; (**c**) 1k3801 at 1400 °C and 26 GPa; (**d**) 5k4195 at 1400 °C and 27 GPa; (**e**) Phase diagrams in MgO-Al_2O_3-H_2O ternary systems. CF = calcium ferrite-type phase; Cor = corundum; Per = periclase; δ = δ-AlOOH phase; Mag = magnesite; SM = starting material

consistent with the spectra of Mg-doped corundum (Supplementary material 1: Fig. S7) (Fukatsu et al. 2003; Jollands et al. 2023). Due to the small crystal size, FTIR spectra of periclase and δ-AlOOH were not measured. Litasov (2010) reported OH-stretching bands in periclase at 3299, 3308, and 3474 cm^{-1}, with the band at 3474 cm^{-1} being notably weak. δ-AlOOH exhibits no significant absorption peaks above 2500 cm^{-1} (Kagi et al. 2010). Thus, the FTIR spectra of the CF phase included none of these phases or contained them in negligible amounts.

The water content of CF phase ranges from 65 to 99 ppm wt in different crystals (Table S2). The average water contents synthesized at 1500, 1700, and 1900 °C were 87(11), 86(11), and 73(5) ppm wt, respectively (Fig. 8), indicating a slight decrease with temperature. Note that broad bands at 3000–3400 cm^{-1} were not consistently observed across different crystals (Supplementary material 1: Fig. S5). When we excluded the bands at 3000–3400 cm^{-1}, the calculated water contents became 10–20 ppm wt lower. We also measured the water content of a corundum crystal, which was estimated to be 1950 ppm wt (Jollands et al. 2023). This excludes the possibility of water-leaking from the capsules and supports the low water contents of CF crystals. Thus, our data are the first report of precise detection of water in CF phase and suggest limited water solubility of CF phase. No FTIR data were obtained at 26–32 GPa and 1200–1400 °C in this study due to the small grain sizes (1–10 μm) caused by additional phases of δ-AlOOH and periclase. However, it is likely that these CF phases also have limited water contents or even lower than those at higher temperatures due to formation of δ-AlOOH and no excess fluid, causing a possible strong water partitioning to δ-AlOOH (e.g. Ishii et al. 2022 d; 2024).

Previous studies have identified a relationship between O–O distance and the frequency of OH stretching peaks in minerals with hydrogen bonds (Libowitzky 2015). The CF phase, despite sharing the same space group (*Pnma*) as bridgmanite, contains four inequivalent O^{2-} sites (Ishii et al. 2018b; Yamada et al. 2018). This structural feature provides at least six different potential positions for hydrogen bonding, which may account for the

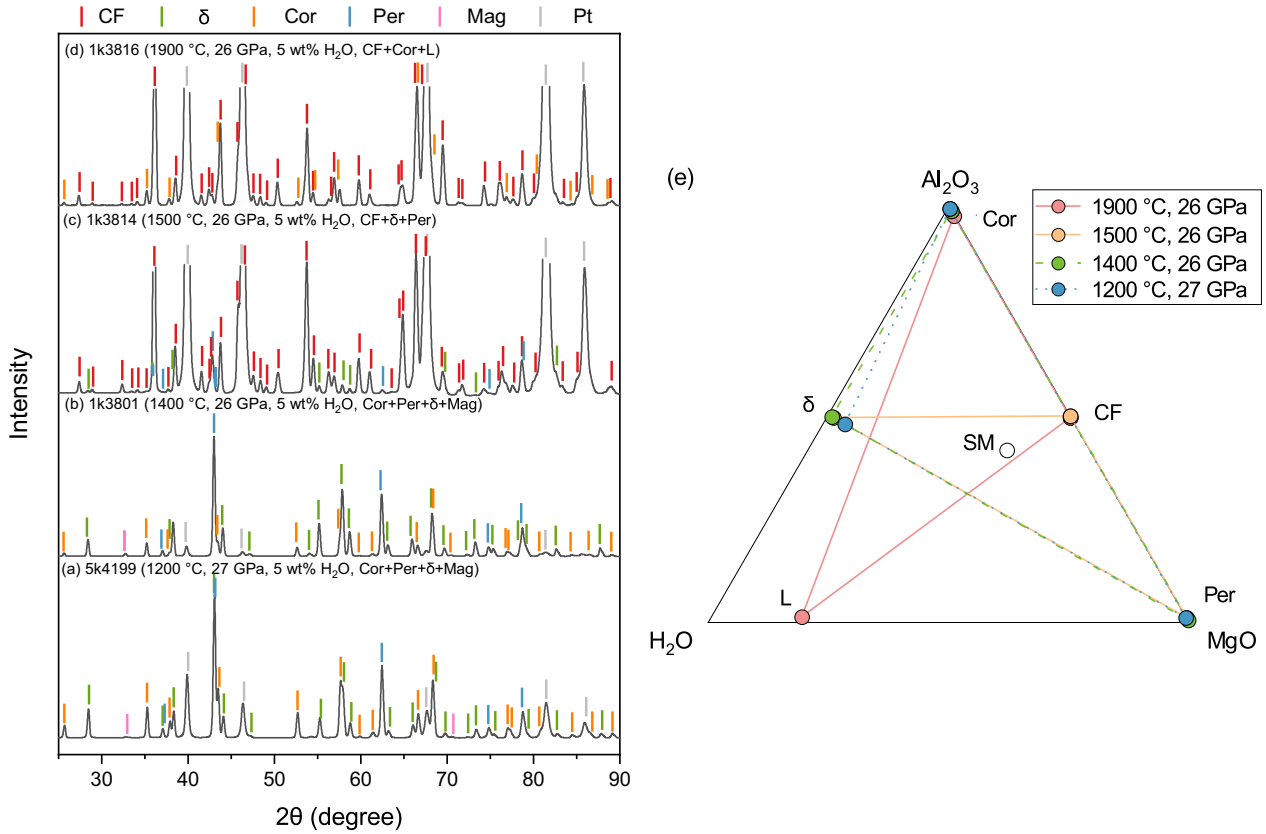

Fig. 5 XRD profiles and phase diagrams of the recovered samples from different runs in 5 wt% H_2O system. (**a**) 5k4199 at 1200 °C and 27 GPa; (**b**) 1k3801 at 1400 °C and 26 GPa; (**c**) 1k3814 at 1500 °C and 26 GPa; (**d**) 1 k 3816 at 1900 °C and 26 GPa; (**e**) Phase diagrams in MgO-Al_2O_3-H_2O ternary systems. CF = calcium ferrite-type phase; Cor = corundum; Per = periclase; δ = δ-AlOOH phase; Mag = magnesite; L = melt; SM = starting material

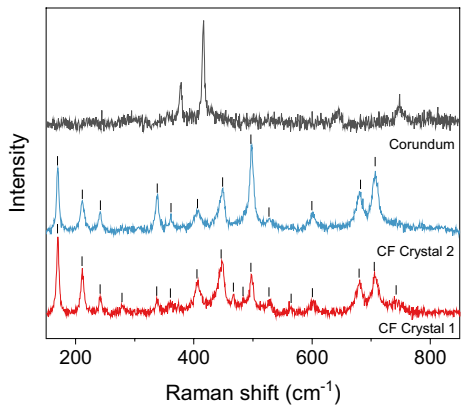

Fig. 6 Representative Raman spectra of recovered samples from the run 1k3791 (26 GPa and 1700 °C in the 5 wt% H_2O system) at 150–850 cm^{-1}

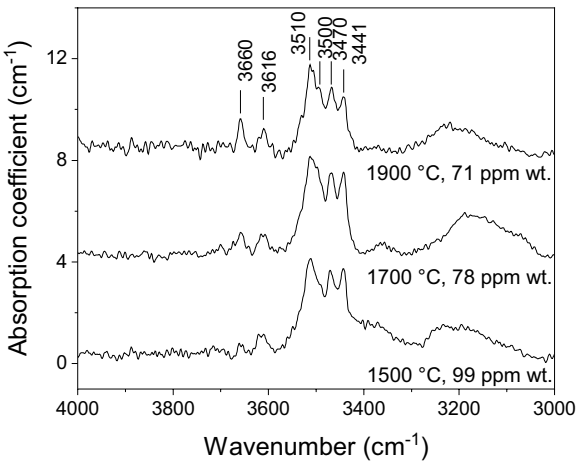

Fig. 7 Representative unpolarized FTIR spectra of $MgAl_2O_4$ CF phase single crystals synthesized at 26 GPa and 1500–1900 °C. The baseline has been subtracted and the spectra are normalized to 1 cm

complex and multiple OH stretching peaks observed in the FTIR spectra. Similar multiple peaks related to different O^{2-} sites have also been observed in hydrous wadsleyite (Deon et al. 2010). Notably, $MgAl_2O_4$ spinel, the low-pressure form of CF phase, was also found to be nearly anhydrous (Bromiley et al. 2010; Lenaz et al. 2008). However, non-stoichiometric defect spinel can contain

several hundred ppm water, likely due to partial coupling of interstitial hydrogen with cation vacancies or Mg–Al disorder on tetrahedral sites (Bromiley et al. 2010). While the small water content in CF phase crystals identified in this study makes it challenging to determine the exact location of hydrogen, it is likely incorporated through oxygen vacancies to compensate for charge imbalance, as mentioned above.

4 Implications

4.1 Stability of CF phase in basaltic crust

As mentioned above, pyrolitic lower-mantle minerals generally have limited water solubility, up to 0.1 wt% (Bolfan-Casanova et al. 2003; Fu et al. 2019; Liu et al. 2021). Therefore, geochemical observations of ocean island basalts with relatively high-water contents (Hirschmann 2006) could be originated from subducted crustal materials. Dry basaltic crusts in the lower mantle consist of bridgmanite, a silica phase, CF phase, davemaoite, and NAL phase (Ishii et al. 2019, 2022c; Ono et al. 2001; Perrillat et al. 2006; Ricolleau et al. 2010). On the other hand, hydrous basaltic crusts with 2–3.5 wt% H_2O in the lower mantle showed a distinct mineral assemblage, consisting of Al-rich hydrous phase H, bridgmanite, davemaoite, ferropericlase, and stishovite with Na depletion together with fluid at relatively low temperatures of 1000–1200 °C (Supplementary material 1: Fig. S1) (Liu et al. 2019). Our study demonstrated that CF-type $MgAl_2O_4$ is stable below 5 wt% H_2O and at relatively high temperatures above 26 GPa and 1500 °C after dehydration of Al-rich hydrous phase H. Therefore, the above mineral assemblage reported in Liu et al. (2019) can change to Na-depleted $MgAl_2O_4$-rich CF phase-bearing assemblage at higher temperatures through the reaction between Al-rich hydrous phase H and ferropericlase as Al-rich hydrous phase H dehydrates as discussed earlier. Further investigation of the phase relations of the hydrous basalts at higher temperatures is necessary to determine the proportion and chemical composition, especially Fe and Si contents, of CF phase. Nevertheless, it is likely that $MgAl_2O_4$-rich CF phase should appear in this environment because of the limited solubility of Fe and Si into the CF phase due to no endmember components such as Mg_2SiO_4 and $FeAl_2O_4$ (Kojitani et al. 2007; Schollenbruch et al. 2009).

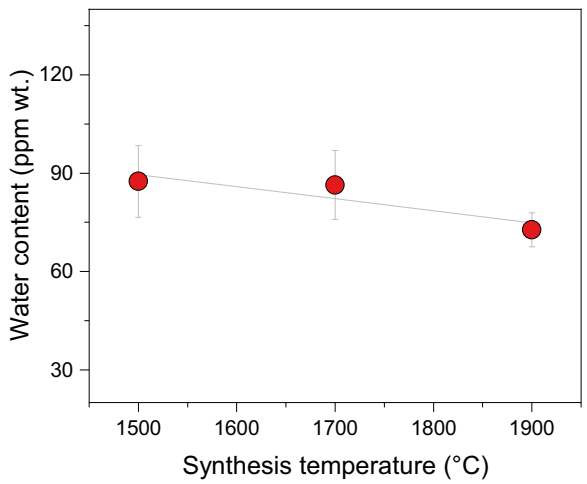

Fig. 8 Average water contents of $MgAl_2O_4$ CF phase at different temperatures and a constant pressure of 26 GPa. Red circles: average water contents at each temperature

These findings suggest that the stability of the CF phase in water-bearing systems in the top lower mantle is primarily controlled by water content and temperature. In regions with a water content less than 5 wt%, the $MgAl_2O_4$-rich CF phase can crystallize while it is not stable at relatively low temperatures in top lower-mantle depths due to the stability of Al-rich hydrous phases, as observed in this study. In such a region, other phases such as bridgmanite and stishovite remain nearly anhydrous (Ishii et al. 2022b, 2022 d; Liu et al. 2021). $MgAl_2O_4$-rich CF phase will stabilize in the warm part of the subducting slab heated by the high-temperature average lower mantle.

4.2 Water transport and water reservoir in the lower mantle

The subducted slab can contain abundant hydrous minerals, such as serpentine, formed through the hydrothermal alteration by seawater or fluids rising from underlying mantle plumes and such alternations can happen even into the slab core (Keppler et al. 2024; Ohtani and Ishii 2024). Water stored in these hydrous minerals will be released at their dehydration temperatures from the slab and move upwards due to its low density. The low water solubility of CF phase observed in this study indicates that the most released water at least uppermost lower mantle conditions likely partitions into aluminous silica minerals and probably davemaoite in the basaltic crust layer because of limited water solubility of other slab-constituent minerals (Chen et al. 2020; Murakami et al. 2002; Ishii et al. 2022b). Consequently, water will be mainly kept in basaltic crusts down to the core-mantle boundary and can return to the shallower parts through upwelling hot plumes (Ishii et al. 2022b; Tsutsumi et al. 2024).

4.3 Possible influence of CF phase on physical properties of the lower mantle

Nearly dry CF phase could exist widely in crustal lithologies and contribute to the shear wave splitting observed at such depths due to its significant elastic anisotropy

(Criniti et al. 2025; Kawai and Tsuchiya 2012; Yin et al. 2012). A recent study revealed that dry CF phase can work as an effective thermal insulator (relatively low thermal conductor), suggesting thermally insulating block by basalt-accumulated regions at the lowermost mantle (Hsieh et al. 2025). Although we found that CF phase shows limited water solubility, such small amounts of water might further reduce its thermal conductivity. By the strong water partitioning to aluminous silica due to other nearly dry lower-mantle minerals, the transition pressure from stishovite to $CaCl_2$-type phase is lowered (Criniti et al. 2023; Zhang et al. 2022), potentially explaining the shallowest high-density and low-shear-wave-velocity seismic scatters around 700 km (e.g. Kaneshima 2016). In addition, in minerals in the Earth's interior, even small water contents (ten to hundreds of ppm) can strongly influence the electrical conductivity (e.g. clinopyroxene) (Yang et al. 2011). Therefore, further investigation of the physical properties of CF phase using obtained single crystals would provide better understanding of the structure and dynamics in the lower mantle.

5 Conclusions

We conducted high-pressure experiments using a Kawai-type multi-anvil press to investigate the stability and water solubility of CF-type $MgAl_2O_4$ under hydrous conditions at 26–32 GPa and 1200–1900 °C. Our results indicate that the CF phase is unstable in systems with water content exceeding 10 wt%. Water solubility measurements by FTIR reveal that the CF phase contains less than 100 ppm wt water, suggesting it is not a major carrier or reservoir of water in the topmost lower mantle. Based on our findings and previous studies, nearly dry $MgAl_2O_4$-rich CF phase likely forms in warmer regions of subducting hydrous crustal materials through reactions between low temperature phases of Al-rich hydrous phase H and ferropericlase. The limited water solubility of the CF phase and most other slab-constituent minerals indicates the most water will be partitioned into aluminous silica minerals after Al-rich hydrous phase H dehydrates. This supports seismic scatterers at the shallow lower mantle are caused by the phase transition of highly hydrated aluminous stishovite and main water carriers and reservoirs in the lower mantle are hydrous aluminous silica minerals.

Abbreviations

CF Calcium ferrite-type phase
NAL New hexagonal aluminous phase
FTIR Fourier transform infrared spectroscopy

Supplementary Information

The online version contains supplementary material available at https://doi.org/10.1186/s40645-025-00702-w.

Additional file 1.

Acknowledgements

We thank K. Lau for FTIR measurement, N.M. Kondo for EPMA measurement, J. Zhu and J. He for SEM observation and EDS measurement at IPM. We also thank two anonymous reviewers for their constructive comments.

Author contributions

TI proposed the topic, conceived and designed the study. XZ and TI carried out the high-pressure experimental study. XZ and IM measured Raman spectra of recovered samples. XZ measured and analyzed FTIR spectra and micro-focus XRD data of recovered samples. XZ wrote the original draft and revised it by including inputs from TI and IM. All authors read and approved the final manuscript.

Funding

This work was supported by JSPS KAKENHI Grants (Numbers 23 K19067 and 24 K00735) to TI. This work was supported by Grant for Basic Science Research Projects of the Sumitomo Foundation (Grant Number, 2300644), the Okayama University Female Staff Support Grant, and JSPS KAKENHI Grants (Number 24 K17147) to IM. This work was supported by the Joint Use Program at IPM (Project Number I23-013) and Program of China Scholarship Council (No. 202306340150) to XZ.

Availability of data and materials

The dataset(s) supporting the conclusions of this article is(are) included within the article (and its additional file(s)).

Declarations

Competing interests

The authors declare that they have no competing interest.

Received: 16 January 2025 Accepted: 6 April 2025
Published online: 12 May 2025

References

Akaogi M, Ishii T, Yamaura K (2024) Post-spinel-type AB_2O_4 high-pressure phases in geochemistry and materials science. Commun Chem 7(1):189. https://doi.org/10.1038/s42004-024-01278-0

Anderson OL, Isaak DG, Yamamoto S (1989) Anharmonicity and the equation of state for gold. J Appl Phys 65(4):1534–1543. https://doi.org/10.1063/1.342969

Andrault D, Bolfan-Casanova N (2022) Mantle rain toward the Earth's surface: a model for the internal cycle of water. Phys Earth Planet Inter 322:106815. https://doi.org/10.1016/j.pepi.2021.106815

Bercovici D, Karato SI (2003) Whole-mantle convection and the transition-zone water filter. Nature 425(6953):39–44. https://doi.org/10.1038/nature01918

Bolfan-Casanova N, Keppler H, Rubie DC (2003) Water partitioning at 660 km depth and evidence for very low water solubility in magnesium silicate perovskite. Geophys Res Lett. https://doi.org/10.1029/2003gl017182

Bromiley GD, Nestola F, Redfern SAT, Zhang M (2010) Water incorporation in synthetic and natural $MgAl_2O_4$ spinel. Geochim Cosmochim Acta 74(2):705–718. https://doi.org/10.1016/j.gca.2009.10.015

Chanyshev A, Ishii T, Bondar D, Bhat S, Kim EJ, Farla R, Nishida K, Liu Z, Wang L, Nakajima A, Yan B, Tang H, Chen Z, Higo Y, Tange Y, Katsura T (2022) Depressed 660-km discontinuity caused by akimotoite-bridgmanite transition. Nature 601(7891):69–73. https://doi.org/10.1038/s41586-021-04157-z

Chen H, Leinenweber K, Prakapenka V, Prescher C, Meng Y, Bechtel H, Kunz M, Shim SH (2020) Possible H_2O storage in the crystal structure of $CaSiO_3$

perovskite. Phys Earth Planet Inter. https://doi.org/10.1016/j.pepi.2019.106412
Criniti G, Ishii T, Kurnosov A, Glazyrin K, Ballaran TB (2023) High-pressure phase transition and equation of state of hydrous Al-bearing silica. Am Mineral 108(8):1558–1568. https://doi.org/10.2138/am-2022-8546
Criniti G, Boffa Ballaran T, Kurnosov A, Ishii T, Rogmann E-M, Glazyrin K, Fedotenko T, Frost DJ (2025) Effect of chemistry on the compressibility and high-pressure structural evolution of the $CaFe_2O_4$-type aluminous silicate phase. Phys Earth Planet Inter. https://doi.org/10.1016/j.pepi.2025.107331
Deon F, Koch-Muller M, Rhede D, Gottschalk M, Wirth R, Thomas SM (2010) Location and quantification of hydroxyl in wadsleyite: New insights. Am Mineral 95(2–3):312–322. https://doi.org/10.2138/am.2010.3267
Enomoto A, Kojitani H, Akaogi M, Miura H, Yusa H (2009) High-pressure transitions in $MgAl_2O_4$ and a new high-pressure phase of $Mg_2Al_2O_5$. J Solid State Chem 182(2):389–395. https://doi.org/10.1016/j.jssc.2008.11.015
Fu S, Yang J, Si K, Vasiliev A, Presniakov MY, Gavriliuk AG, Ivanova AG, Hauri EH, Okuchi T, Purevjav N, Lin JF (2019) Water concentration in single-crystal (Al, Fe)-bearing bridgmanite grown from the hydrous melt: Implications for dehydration melting at the topmost lower mantle. Geophys Res Lett 46(17–18):10346–10357. https://doi.org/10.1029/2019gl084630
Fukatsu N, Kurita N, Oka Y, Yamamoto S (2003) Incorporation of hydrogen into magnesium-doped α-alumina. Solid State Ionics 162–163:147–159. https://doi.org/10.1016/s0167-2738(03)00218-2
Green DH, Hibberson WO, Rosenthal A, Kovács I, Yaxley GM, Falloon TJ, Brink F (2014) Experimental study of the influence of water on melting and phase assemblages in the upper mantle. J Petrol 55(10):2067–2096. https://doi.org/10.1093/petrology/egu050
Hack AC, Thompson AB (2011) Density and viscosity of hydrous magmas and related fluids and their role in subduction zone processes. J Petrol 52(7–8):1333–1362. https://doi.org/10.1093/petrology/egq048
Hirschmann MM (2006) Water, melting, and the deep Earth H_2O cycle. Annu Rev Earth Planet Sci 34(1):629–653. https://doi.org/10.1146/annurev.earth.34.031405.125211
Hsieh WP, Ishii T, Deschamps F, Tsao YC, Chang JW, Criniti G (2025) Reduced thermal conductivity of hydrous aluminous silica and calcium ferrite-type phase promote water transportation to earth's deep mantle. J Geophys Res Solid Earth. https://doi.org/10.1029/2024jb030704
Irifune T, Fujino K, Ohtani E (1991) A new high-pressure form of $MgAl_2O_4$. Nature 349(6308):409–411. https://doi.org/10.1038/349409a0
Irifune T, Ringwood AE, Hibberson WO (1994) Subduction of continental crust and terrigenous and pelagic sediments: an experimental study. Earth Planet Sci Lett 126(4):351–368. https://doi.org/10.1016/0012-821x(94)90117-1
Irifune T, Naka H, Sanehira T, Inoue T, Funakoshi K (2002) In situ X-ray observations of phase transitions in $MgAl_2O_4$ spinel to 40 GPa using multianvil apparatus with sintered diamond anvils. Phys Chem Miner 29(10):645–654. https://doi.org/10.1007/s00269-002-0275-1
Irifune T, Shinmei T, McCammon CA, Miyajima N, Rubie DC, Frost DJ (2010) Iron partitioning and density changes of pyrolite in Earth's lower mantle. Science 327(5962):193–195. https://doi.org/10.1126/science.1181443
Ishii T, Kojitani H, Akaogi M (2011) Post-spinel transitions in pyrolite and Mg_2SiO_4 and akimotoite–perovskite transition in $MgSiO_3$: Precise comparison by high-pressure high-temperature experiments with multi-sample cell technique. Earth Planet Sci Lett 309(3–4):185–197. https://doi.org/10.1016/j.epsl.2011.06.023
Ishii T, Kojitani H, Akaogi M (2012) High-pressure phase transitions and subduction behavior of continental crust at pressure–temperature conditions up to the upper part of the lower mantle. Earth Planet Sci Lett 357–358:31–41. https://doi.org/10.1016/j.epsl.2012.09.019
Ishii T, Shi L, Huang R, Tsujino N, Druzhbin D, Myhill R, Li Y, Wang L, Yamamoto T, Miyajima N, Kawazoe T, Nishiyama N, Higo Y, Tange Y, Katsura T (2016) Generation of pressures over 40 GPa using Kawai-type multi-anvil press with tungsten carbide anvils. Rev Sci Instrum 87(2):024501. https://doi.org/10.1063/1.4941716
Ishii T, Yamazaki D, Tsujino N, Xu F, Liu Z, Kawazoe T, Yamamoto T, Druzhbin D, Wang L, Higo Y, Tange Y, Yoshino T, Katsura T (2017) Pressure generation to 65 GPa in a Kawai-type multi-anvil apparatus with tungsten carbide anvils. High Pressure Res 37(4):507–515. https://doi.org/10.1080/08957959.2017.1375491
Ishii T, Kojitani H, Akaogi M (2018a) Phase relations and mineral chemistry in pyrolitic mantle at 1600–2200 °C under pressures up to the uppermost lower mantle: phase transitions around the 660-km discontinuity and dynamics of upwelling hot plumes. Phys Earth Planet Inter 274:127–137. https://doi.org/10.1016/j.pepi.2017.10.005
Ishii T, Sakai T, Kojitani H, Mori D, Inaguma Y, Matsushita Y, Yamaura K, Akaogi M (2018b) High-pressure phase relations and crystal structures of postspinel phases in MgV_2O_4, FeV_2O_4, and $MnCr_2O_4$: Crystal chemistry of AB_2O_4 postspinel compounds. Inorg Chem 57(11):6648–6657. https://doi.org/10.1021/acs.inorgchem.8b00810
Ishii T, Kojitani H, Akaogi M (2019) Phase relations of Harzburgite and MORB up to the uppermost lower mantle conditions: precise comparison with pyrolite by multisample cell high-pressure experiments with implication to dynamics of subducted slabs. J Geophys Res: Solid Earth 124(4):3491–3507. https://doi.org/10.1029/2018jb016749
Ishii T, Criniti G, Bykova E, Dubrovinsky L, Katsura T, Arii H, Kojitani H, Akaogi M (2021) High-pressure syntheses and crystal structure analyses of a new low-density $CaFe_2O_4$-related and $CaTi_2O_4$-type $MgAl_2O_4$ phases. Am Mineral 106(7):1105–1112. https://doi.org/10.2138/am-2021-7619
Ishii T, Chanyshev A, Katsura T (2022) A new approach determining a phase transition boundary strictly following a definition of phase equilibrium: An example of the post-spinel transition in Mg_2SiO_4 system. Minerals. https://doi.org/10.3390/min12070820
Ishii T, Criniti G, Ohtani E, Purevjav N, Fei H, Katsura T, Mao HK (2022b) Superhydrous aluminous silica phases as major water hosts in high-temperature lower mantle. Proc Natl Acad Sci U S A 119(44):e2211243119. https://doi.org/10.1073/pnas.2211243119
Ishii T, Miyajima N, Criniti G, Hu Q, Glazyrin K, Katsura T (2022) High pressure-temperature phase relations of basaltic crust up to mid-mantle conditions. Earth Planet Sci Lett. https://doi.org/10.1016/j.epsl.2022.117472
Ishii T, Ohtani E, Shatskiy A (2022) Aluminum and hydrogen partitioning between bridgmanite and high-pressure hydrous phases: Implications for water storage in the lower mantle. Earth Planet Sci Lett. https://doi.org/10.1016/j.epsl.2022.117441
Ishii T, Criniti G, Wang X, Glazyrin K, Boffa Ballaran T (2023a) Synthesis and structural analysis of $CaFe_2O_4$-type single crystals in the $NaAlSiO_4$-$MgAl_2O_4$-Fe_3O_4 system. Am Mineral 108(1):217–221. https://doi.org/10.2138/am-2022-8748
Ishii T, Frost DJ, Kim EJ, Chanyshev A, Nishida K, Wang B, Ban R, Xu J, Liu J, Su X, Higo Y, Tange Y, Mao H-k, Katsura T (2023b) Buoyancy of slabs and plumes enhanced by curved post-garnet phase boundary. Nat Geosci 16(9):828–832. https://doi.org/10.1038/s41561-023-01244-w
Ishii T, Criniti G, Purevjav N, Katsura T, Ohtani E (2024) Hydrogen partitioning between stishovite and hydrous phase δ: implications for water cycle and distribution in the lower mantle. Progress Earth Planet Sci. https://doi.org/10.1186/s40645-024-00615-0
Jollands MC, Jin S, Curti M, Guillaumet M, Béneut K, Giura P, Balan E (2023) Vibrational properties of OH groups associated with divalent cations in corundum (α-Al_2O_3). Eur J Mineral 35(5):873–890. https://doi.org/10.5194/ejm-35-873-2023
Kagi H, Ushijima D, Sano-Furukawa A, Komatsu K, Iizuka R, Nagai T, Nakano S (2010) Infrared absorption spectra of δ-AlOOH and its deuteride at high pressure and implication to pressure response of the hydrogen bonds. J Phys Conf Ser. https://doi.org/10.1088/1742-6596/215/1/012052
Kaneshima S (2016) Seismic scatterers in the mid-lower mantle. Phys Earth Planet Inter 257:105–114. https://doi.org/10.1016/j.pepi.2016.05.004
Kawai K, Tsuchiya T (2012) Phase stability and elastic properties of the NAL and CF phases in the $NaMg_2Al_5SiO_{12}$ system from first principles. Am Mineral 97(2–3):305–314. https://doi.org/10.2138/am.2012.3915
Keppler H, Ohtani E, Yang X (2024) The subduction of hydrogen: deep water cycling, induced seismicity, and plate tectonics. Elements 20(4):229–234. https://doi.org/10.2138/gselements.20.4.229
Kohlstedt DL (2006) The role of water in high-temperature rock deformation. Rev Mineral Geochem 62(1):377–396. https://doi.org/10.2138/rmg.2006.62.16
Kojitani H, Nishimura K, Kubo A, Sakashita M, Aoki K, Akaogi M (2003) Raman spectroscopy and heat capacity measurement of calcium ferrite type $MgAl_2O_4$ and $CaAl_2O_4$. Phys Chem Miner 30(7):409–415. https://doi.org/10.1007/s00269-003-0332-4
Kojitani H, Hisatomi R, Akaogi M (2007) High-pressure phase relations and crystal chemistry of calcium ferrite-type solid solutions in the system $MgAl_2O_4$-Mg_2SiO_4. Am Mineral 92(7):1112–1118. https://doi.org/10.2138/am.2007.2255

Kojitani H, Ishii T, Akaogi M (2012a) Thermodynamic investigation on phase equilibrium boundary between calcium ferrite-type MgAl2O4 and MgO+α-Al2O3. Phys Earth Planet Inter 212–213:100–105. https://doi.org/10.1016/j.pepi.2012.10.002

Kojitani H, Tobbens DM, Akaogi M (2012b) High-pressure Raman spectroscopy, vibrational mode calculation, and heat capacity calculation of calcium ferrite-type $MgAl_2O_4$ and $CaAl_2O_4$. Am Mineral 98(1):197–206. https://doi.org/10.2138/am.2013.4095

Lenaz D, Skogby H, Nestola F, Princivalle F (2008) OH incorporation in nearly pure MgAl2O4 natural and synthetic spinels. Geochim Cosmochim Acta 72(2):475–479. https://doi.org/10.1016/j.gca.2007.10.020

Libowitzky E (2015) Correlation of O-H stretching frequencies and O-H…O hydrogen bond lengths in minerals. Monatshefte Für Chemie/Chem Mon 130(8):1047–1059. https://doi.org/10.1007/bf03354882

Litasov KD (2010) The influence of Al2O3 on the H2O content in periclase and ferropericlase at 25 GPa. Russ Geol Geophys 51(6):644–649. https://doi.org/10.1016/j.rgg.2010.05.005

Litasov K, Ohtani E, Langenhorst F, Yurimoto H, Kubo T, Kondo T (2003) Water solubility in Mg-perovskites and water storage capacity in the lower mantle. Earth Planet Sci Lett 211(1–2):189–203. https://doi.org/10.1016/s0012-821x(03)00200-0

Litasov KD, Kagi H, Shatskiy A, Ohtani E, Lakshtanov DL, Bass JD, Ito E (2007) High hydrogen solubility in Al-rich stishovite and water transport in the lower mantle. Earth Planet Sci Lett 262(3–4):620–634. https://doi.org/10.1016/j.epsl.2007.08.015

Liu Z, Nishi M, Ishii T, Fei H, Miyajima N, Ballaran TB, Ohfuji H, Sakai T, Wang L, Shcheka S, Arimoto T, Tange Y, Higo Y, Irifune T, Katsura T (2017) Phase relations in the system $MgSiO_3$-Al_2O_3 up to 2300 K at lower mantle pressures. J Geophys Res: Solid Earth 122(10):7775–7788. https://doi.org/10.1002/2017jb014579

Liu X, Matsukage KN, Nishihara Y, Suzuki T, Takahashi E (2019) Stability of the hydrous phases of Al-rich phase D and Al-rich phase H in deep subducted oceanic crust. Am Mineral 104(1):64–72. https://doi.org/10.2138/am-2019-6559

Liu Z, Fei H, Chen L, McCammon C, Wang L, Liu R, Wang F, Liu B, Katsura T (2021) Bridgmanite is nearly dry at the top of the lower mantle. Earth Planet Sci Lett. https://doi.org/10.1016/j.epsl.2021.117088

Mao Z, Jacobsen SD, Jiang F, Smyth JR, Holl CM, Frost DJ, Duffy TS (2008) Single-crystal elasticity of wadsleyites, β-Mg2SiO4, containing 037–16.6 wt.% H2O. Earth Planet Sci Lett 266(1–2):78–89. https://doi.org/10.1016/j.epsl.2007.10.045

Marzotto E, Hsieh WP, Ishii T, Chao KH, Golabek GJ, Thielmann M, Ohtani E (2020) Effect of water on lattice thermal conductivity of ringwoodite and its implications for the thermal evolution of descending slabs. Geophys Res Lett. https://doi.org/10.1029/2020gl087607

Murakami M, Hirose K, Yurimoto H, Nakashima S, Takafuji N (2002) Water in Earth's lower mantle. Science 295(5561):1885–1887. https://doi.org/10.1126/science.1065998

Nishi M, Irifune T, Tsuchiya J, Tange Y, Nishihara Y, Fujino K, Higo Y (2014) Stability of hydrous silicate at high pressures and water transport to the deep lower mantle. Nat Geosci 7(3):224–227. https://doi.org/10.1038/ngeo2074

Nishiyama N, Yagi T (2003) Phase relation and mineral chemistry in pyrolite to 2200°C under the lower mantle pressures and implications for dynamics of mantle plumes. J Geophys Res Solid Earth. https://doi.org/10.1029/2002jb002216

Ohtani E, Ishii T (2024) Role of water in dynamics of slabs and surrounding mantle. Progress Earth Planet Sci. https://doi.org/10.1186/s40645-024-00670-7

Ono S, Ito E, Katsura T (2001) Mineralogy of subducted basaltic crust (MORB) from 25 to 37 GPa, and chemical heterogeneity of the lower mantle. Earth Planet Sci Lett 190(1–2):57–63. https://doi.org/10.1016/s0012-821x(01)00375-2

Paterson MS (1982) The determination of hydroxyl by infrared absorption in quartz, silicate glasses and similar materials. Bull Minér 105(1):20–29. https://doi.org/10.3406/bulmi.1982.7582

Pearson DG, Brenker FE, Nestola F, McNeill J, Nasdala L, Hutchison MT, Matveev S, Mather K, Silversmit G, Schmitz S, Vekemans B, Vincze L (2014) Hydrous mantle transition zone indicated by ringwoodite included within diamond. Nature 507(7491):221–224. https://doi.org/10.1038/nature13080

Perrillat J-P, Ricolleau A, Daniel I, Fiquet G, Mezouar M, Guignot N, Cardon H (2006) Phase transformations of subducted basaltic crust in the upmost lower mantle. Phys Earth Planet Inter 157(1–2):139–149. https://doi.org/10.1016/j.pepi.2006.04.001

Purevjav N, Fei H, Ishii T, Criniti G, Lin Y, Mao HK, Katsura T (2024) Temperature dependence of H2O solubility in Al-free stishovite. Geophys Res Lett. https://doi.org/10.1029/2023gl104029

Ricolleau A, Perrillat J-P, Fiquet G, Daniel I, Matas J, Addad A, Menguy N, Cardon H, Mezouar M, Guignot N (2010) Phase relations and equation of state of a natural MORB: implications for the density profile of subducted oceanic crust in the Earth's lower mantle. J Geophys Res. https://doi.org/10.1029/2009jb006709

Schollenbruch K, Woodland AB, Frost DJ (2009) The stability of hercynite at high pressures and temperatures. Phys Chem Miner 37(3):137–143. https://doi.org/10.1007/s00269-009-0317-z

Tsuchiya T (2003) First-principles prediction of the P-V-T equation of state of gold and the 660-km discontinuity in Earth's mantle. J Geophys Res Solid Earth. https://doi.org/10.1029/2003jb002446

Tsutsumi Y, Sakamoto N, Hirose K, Tagawa S, Umemoto K, Ohishi Y, Yurimoto H (2024) Retention of water in subducted slabs under core–mantle boundary conditions. Nat Geosci 17(7):697–704. https://doi.org/10.1038/s41561-024-01464-8

Wang D, Mookherjee M, Xu Y, Karato S (2006) The effect of water on the electrical conductivity of olivine. Nature 443(7114):977–980. https://doi.org/10.1038/nature05256

Yamada H, Matsui Y, Ito E (2018) Crystal-chemical characterization of $NaAlSiO_4$ with the $CaFe_2O_4$ structure. Mineral Mag 47(343):177–181. https://doi.org/10.1180/minmag.1983.047.343.07

Yang X, Keppler H, McCammon C, Ni H, Xia Q, Fan Q (2011) Effect of water on the electrical conductivity of lower crustal clinopyroxene. J Geophys Res. https://doi.org/10.1029/2010jb008010

Yin K, Zhou H, Huang Q, Sun Y, Xu S, Lu X (2012) First-principles study of high-pressure elasticity of CF- and CT-structure MgAl2O4. Geophys Res Lett. https://doi.org/10.1029/2011gl050229

Yokoo M, Kawai N, Nakamura KG, Kondo K-i, Tange Y, Tsuchiya T (2009) Ultrahigh-pressure scales for gold and platinum at pressures up to 550 GPa. Phys Rev B. https://doi.org/10.1103/PhysRevB.80.104114

Zhang Y, Fu S, Si Karato, Okuchi T, Chariton S, Prakapenka VB, Lin JF (2022) Elasticity of hydrated al-bearing stishovite and post-stishovite: implications for understanding regional seismic vs anomalies along subducting slabs in the lower mantle. J Geophys Res Solid Earth. https://doi.org/10.1029/2021jb023170

Zhang X, Wei W, Li L, Yu Y, Mao Z (2024) High-pressure single-crystal elasticity of corundum: Implication for multiple seismic structure of 660-km discontinuity. Phys Earth Planet Inter. https://doi.org/10.1016/j.pepi.2023.107134

Publisher's Note